Ergodic and nonergodic processes coexist in the plasma membrane as observed by single-molecule tracking

Aubrey V. Weigel[a], Blair Simon[b], Michael M. Tamkun[c,d], and Diego Krapf[a,b,1]

[a]School of Biomedical Engineering, Colorado State University, Fort Collins, CO 80523; [b]Department of Electrical and Computer Engineering, Colorado State University, Fort Collins, CO 80523; [c]Department of Biomedical Sciences, Colorado State University, Fort Collins, CO 80523; and [d]Department of Biochemistry and Molecular Biology, Colorado State University, Fort Collins, CO 80523

Edited* by Jennifer Lippincott-Schwartz, National Institutes of Health, Bethesda, MD, and approved February 23, 2011 (received for review October 31, 2010).

Diffusion in the plasma membrane of living cells is often found to display anomalous dynamics. However, the mechanism underlying this diffusion pattern remains highly controversial. Here, we study the physical mechanism underlying Kv2.1 potassium channel anomalous dynamics using single-molecule tracking. Our analysis includes both time series of individual trajectories and ensemble averages. We show that an ergodic and a nonergodic process coexist in the plasma membrane. The ergodic process resembles a fractal structure with its origin in macromolecular crowding in the cell membrane. The nonergodic process is found to be regulated by transient binding to the actin cytoskeleton and can be accurately modeled by a continuous-time random walk. When the cell is treated with drugs that inhibit actin polymerization, the diffusion pattern of Kv2.1 channels recovers ergodicity. However, the fractal structure that induces anomalous diffusion remains unaltered. These results have direct implications on the regulation of membrane receptor trafficking and signaling.

anomalous subdiffusion | Brownian motion | continuous time random walk | single-particle tracking

The plasma membrane is a highly complex system with a dynamic organization required to maintain many fundamental processes that include signal transduction, receptor recognition, endocytic transport, and cell–cell adhesion. The study of the diffusion pattern of transmembrane proteins and lipids grants biophysical information on membrane organization, structure, and dynamics. In particular, single-molecule tracking provides insight into the interaction of membrane proteins with their surroundings. Stochastic molecular transport is described by the probability distribution of displacements and how it evolves over time. This distribution is called a propagator, and in the case of Brownian motion it is Gaussian. Diffusion processes that deviate from Brownian motion are considered anomalous, and they involve propagators that may or may not be Gaussian. For example, diffusion in a fractal has a stretched Gaussian propagator (1).

Experimental and theoretical work suggests there is a correlation between macromolecular crowding and anomalous diffusion (2–4). However, the mechanism behind hindered diffusion in living cells remains controversial. Several models have been proposed, including membrane compartmentalization, receptor and cytoskeleton binding, and membrane heterogeneity (lipid rafts). Particle trajectories are frequently characterized by their mean square displacement (MSD) (5). A Brownian particle in a 2D space yields an MSD $\langle \Delta r^2(t) \rangle = 4Dt$. However, in many systems the MSD scales as a sublinear power law, indicating anomalous diffusion. In general $\langle \Delta r^2(t) \rangle \propto t^{\gamma}$, where γ is the anomaly exponent. Anomalous subdiffusion is manifested by a characteristic exponent $\gamma < 1$, and anomalous superdiffusion by $\gamma > 1$.

Two biologically relevant processes are recognized to induce anomalous subdiffusion in the plasma membrane: (*i*) transient immobilization and (*ii*) geometrical inhomogeneities. The former can be modeled by a continuous-time random walk (CTRW) with a heavy-tailed waiting-time probability distribution function (6). Besides giving rise to anomalous diffusion, a CTRW is nonergodic—in other words, the temporal average of a long trajectory differs from the ensemble average (7–9). Molecular crowding and fence-like structures are responsible for space inhomogeneities that can give rise to a hierarchy of cul-de-sacs in the molecule path. One well-known model of such a scenario is given by the percolation cluster, which may be regarded as a random fractal (10). Diffusion on a fractal is a stationary process and thus ergodic. Both a CTRW and diffusion on a fractal have non-Gaussian propagators. A third anomalous diffusion model is fractional Brownian motion (FBM) (11–13), characterized by long-time correlations. Contrary to the previously discussed models, FBM has a Gaussian propagator with a time-dependent diffusion coefficient. Different methods such as p variation tests for categorizing diffusion are emerging (14, 15). Currently these tests are still too simple to handle cases like the one presented here, where more than a single mechanism may be involved. Analysis of the propagator $P(r)$ can provide information on the anomalous behavior, but elucidating the underlying mechanism from the MSD or the propagator alone is an insurmountable task (Fig. S1).

It is common to use the cumulative distribution function ($\mathrm{CDF}(r^2,t_{\mathrm{lag}}) = \int_0^r P(r')2\pi r' dr'$ in two dimensions) to distinguish between normal and anomalous diffusion (16, 17). Within this formalism, Brownian motion yields a single-exponential curve

$$\mathrm{CDF}(r^2,t_{\mathrm{lag}}) = 1 - \exp(-r^2/r_0^2) \quad [1]$$

where ${r_0}^2$ is the MSD in a time t_{lag}. On the other hand, assuming a two-component mobility leads to a double-exponential curve

$$\mathrm{CDF}(r^2,t_{\mathrm{lag}}) = 1 - [w\exp(-r^2/r_1^2) + (1-w)\exp(-r^2/r_2^2)] \quad [2]$$

where r_1 and r_2 are defined by the diffusion constants of the fast and slow mobility component respectively, $r_i^2 = 4D_i t_{\mathrm{lag}}$, with fractions w and $(1-w)$ (16). This method gives minimal information about the diffusion process, but it provides enough information to identify whether the diffusion pattern is normal or anomalous. Normal diffusion yields w values close to 1 (or zero) in the biexponential fit, but when diffusion becomes anomalous, w approaches 0.5.

Here we report studies on the membrane diffusion of the voltage-gated potassium channel Kv2.1 analyzed by single-particle

Author contributions: M.M.T. and D.K. designed research; A.V.W. performed research; B.S., M.M.T., and D.K. contributed new reagents/analytic tools; A.V.W. and D.K. analyzed data; and D.K. wrote the paper.

The authors declare no conflict of interest.

*This Direct Submission article had a prearranged editor.

[1]To whom correspondence should be addressed: E-mail: krapf@engr.colostate.edu.

This article contains supporting information online at www.pnas.org/lookup/suppl/doi:10.1073/pnas.1016325108/-/DCSupplemental.

tracking. The Kv2.1 channel has an interesting characteristic in that it forms stable clusters 0.5 to 15 μm in size on the membrane of transfected human embryonic kidney (HEK) cells and native neurons. Our previous work suggests that clusters are formed by an actin-based mechanism that corrals mobile channels behind a diffusion barrier (18, 19). We dually label the channels with green fluorescent protein (GFP) and quantum dots (QDs) and track their position with nanometer accuracy using total internal reflection fluorescence microscopy (TIRFM). We acquired 1,015 trajectories, many of them longer than 10 min, to allow the analysis and comparison of both time and ensemble averages. We studied the underlying mechanisms for the observed anomalous diffusion focusing our attention on the CTRW, diffusion on a fractal, and a combination of both. Our findings show that Kv2.1 trajectories are best modeled by a CTRW in a fractal geometry. The implications of these processes are discussed. The CTRW is regulated by the actin cytoskeleton while the geometric inhomogeneities are consistent with macromolecular crowding.

Models for Anomalous Diffusion

CTRW. A CTRW represents energetic disorder that may stem from transient binding (5, 20, 21). In this model, a particle jumps between lattice sites, having a random waiting time at each site with a probability density that scales as $t^{-(\alpha+1)}$. The energy landscape of this process is distinguished by wells with a broad depth distribution that transiently trap the particle. This landscape yields an infinite characteristic waiting-time mean and a finite jump-length mean. Many different physical systems are described by CTRWs (22–26). This behavior is nonergodic and it can only exist away from thermodynamic equilibrium. Despite the complexity of CTRWs, the cause for ergodicity breaking is fairly simple. Generally, a system exhibits ergodicity when the measurement time is long in relation to the characteristic time scale (7). In the CTRW, the experimental time can never reach the characteristic time of the process because the mean waiting time is infinite. Therefore, time averages never approach the ensemble averages, independent of the experimental time. The ensemble-averaged MSD follows a power law t^{α}, but the time-averaged MSD is linear, resembling Fickian diffusion (7–9). However, the time-ensemble-averaged MSD (i.e., averaging over both time and ensemble) exhibits aging behavior (8, 9, 27).

Diffusion on a Fractal. Diffusion on a fractal resembles a random walk in an entangled labyrinth with the walker encountering dead ends on all length scales. Fractal geometries are found in a broad range of structures in nature, and thus the implications of diffusion in fractals are extensive (10, 28). In the cell membrane a fractal structure may appear, for example, when macromolecular crowding reaches the percolation threshold (17, 29). Fractals are characterized by a noninteger dimension d_f, and diffusion in a fractal is found to be subdiffusive with a critical exponent $\beta < 1$. This parameter is related to the fractal dimension of the walk d_w by $\beta = 2/d_w$ (10, 17, 30). Intuitively, the dimension of a random walk in a plane is 2D. However, if $d_w > d_f$ then each site in the fractal is visited by the walker several times before moving on to explore a different region. As in the labyrinth analogy, the walker returns through the same path every time it hits a dead end.

Results

Kv2.1 Diffusion Pattern Is Non-Gaussian and Nonergodic. Fig. 1 shows two-color TIRF images of human embryonic kidney (HEK) cells expressing GFP-Kv2.1 channels, labeled with QDs. Representative QD trajectories are superimposed on the images. All Kv2.1 channels expressed in the cell are conjugated to GFP to provide information on cluster size and location. From GFP photobleaching step analysis (31) we find that Kv2.1 density is 15–70 molecules/μm^2 inside clusters. On the other hand, only one QD is present every 10 clusters. Two distinct channel populations are observed, clustering and freely diffusing channels (18). About 97% of the QDs remain confined to one cluster for the entire experimental time.

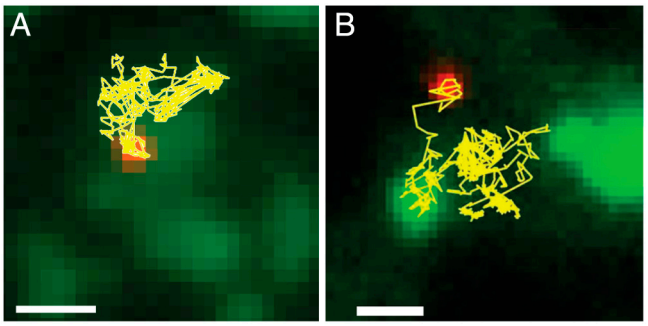

Fig. 1. Overlay image of GFP-tagged Kv2.1 clusters and individual QDs. Kv2.1 clusters are shown in green and QD-tagged channels in red. The trajectories of (*A*) a clustered and (*B*) a nonclustered (free) Kv2.1 channels are shown. Interestingly, the nonclustered channel ignores the compartment perimeters and the channel travels freely into and out of a cluster. Scale bars: 1 μm.

In order to determine whether channel diffusion is normal or anomalous, we constructed the CDFs of all trajectories at numerous time lags and fit the data to monoexponential or biexponential functions using an automated least squares algorithm in MATLAB (16, 32). The analysis of residuals reveals strong systematic deviations from the monoexponential functions. All analyzed CDFs, belonging to both free and clustered channels, fit well to a biexponential form indicating the diffusion pattern is not Gaussian (Fig. 2*A* and Fig. S2). The temporal MSD agrees with these results (Fig. 2*B* and Fig. S3). The diffusion parameter is very broadly distributed, but in almost all free and clustered (at short times) channels the MSD scales as a sublinear power law. The details of the CDF and MSD statistical results are shown in Fig. S4 and Table S1. Besides the fact that a biexponential fit yields better results than a monoexponential one, we use the parameter w in Eq. **2** as an indicator of diffusion anomaly. This parameter is found to be independent of time lag (Fig. 2*C*) and it is 0.5, suggesting all trajectories are anomalous. Normal diffusion would yield w close to zero or one. The clustered channels are analyzed at short times so that the cluster perimeter does not influence our results. The reader is referred to *SI Text*, Fig. S4, and Fig S5 for details on controls including nonclustering Kv1.4 channels and Monte Carlo simulations.

Fig. 2*D* displays distributions of time- and ensemble-averaged MSDs. Temporal MSD distributions are constructed from the individual trajectories. The ensemble MSD distribution is measured by averaging the square displacements of all trajectories occurring at a specific time—e.g., the displacements occurring between 100.0 s and 100.1 s. If the diffusion process were ergodic, both distributions would be similar. However, the temporal MSD is significantly broader than the ensemble MSD for both free and clustered channels. We confirmed that these results are not due to interactions between the QD and the extracellular matrix or the cover slip surface by analyzing the trajectories of GFP-Kv2.1 channels. Because 3% of the Kv2.1 channels do not cluster, we can find individual non-QD-tagged, GFP-Kv2.1 channels freely diffusing outside the clusters. The signal-to-noise ratio and thus the tracking accuracy are poorer than those of QDs, but we are able to track and analyze these channels, following only the GFP signal, as control measurements. Single GFP-Kv2.1 yielded the same CDF, MSD, and distributions of square displacements as the ones found using QDs (Fig. 2*E* and Fig. S2). The median of the effective diffusion constant (i.e., $\langle \Delta r^2 \rangle / 4t_{\mathrm{lag}}$) is fivefold higher in free channels than in clustered channels; but the temporal MSD distribution remains significantly broader than the ensem-

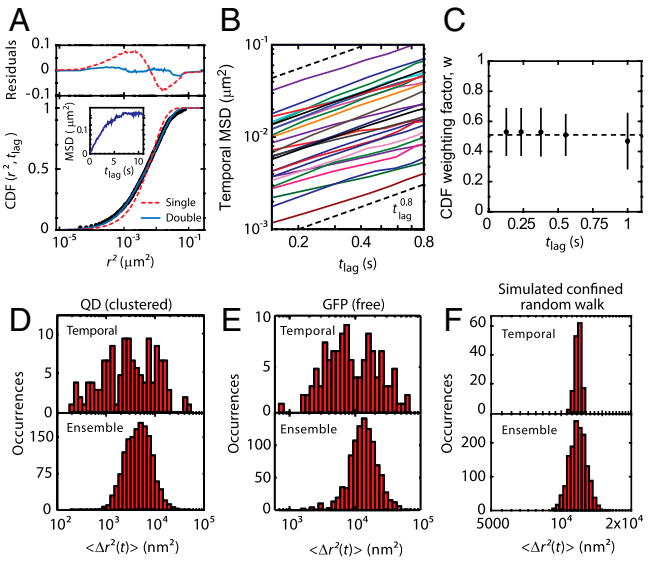

Fig. 2. Statistical analysis of Kv2.1 channel trajectories. (*A*) Square displacement CDF of a representative clustered channel at $t_{lag} = 0.1$ s. Fits to both single-exponential using Eq. **1**, dash red, and biexponential using Eq. **2**, solid blue, are shown together with their respective residuals. The inset is the MSD of this trajectory. (*B*) Log–log plot of the temporal MSD of 26 representative trajectories of clustered channels. The dashed lines scale as $t^{0.8}$ in order to show that the trajectories are sublinear with an exponent equal to or smaller than 0.8. The MSD data for a longer time range is presented in Fig. S3. (*C*) Weighting value of the slow mobility component (w) in Eq. **2** vs. lag time. (*D*) Distribution of MSD values calculated from individual trajectories and ensembles in clustered channels for $t_{lag} = 0.1$ s. (*E*) Control measurements of MSD distribution in GFP-tagged channels without QDs. In order to track individual GFP we analyzed nonclustered channels, which exhibit a five-time higher median effective diffusion constant. (*F*) Distribution of MSD values calculated from simulated confined random walkers.

ble MSD. This effect is seen in both GFP and QD tracking of nonclustered channels. As a control of our averaging algorithms, Fig. 2*F* shows the time and ensemble averages for the simulated confined random walkers. The two distributions are very similar and, as expected from the central limit theorem applied to a Gaussian process, the width of the distribution for the simulated data is $\sigma \propto 1/\sqrt{N}$, where N is the number of independent variables.

In order to compare the diffusion pattern to the CTRW model predictions, we examined the time-ensemble-averaged MSD (TEA-MSD) for all data at different lag times. The TEA-MSD was obtained by applying an additional ensemble average to the temporal MSD. Fig. 3*A* shows the MSD vs. the length of the trajectory, which was measured by truncating the experimental data at a time T and performing a temporal average (i.e., a moving average). The TEA-MSD fluctuated for short times (due to

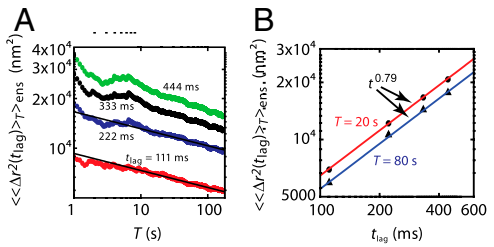

Fig. 3. Time-ensemble-averaged MSD of clustered Kv2.1 channels. (*A*) The MSD is plotted against total time—i.e., the time used in the moving average. The straight lines show a power law fit MSD $\sim T^{\alpha-1}$, with a slope $\alpha - 1 = -0.10$. (*B*) The MSDs for total times 20 s and 80 s are plotted against lag time. At both total times the MSDs exhibit the same subdiffusion critical exponent.

small number statistics), but it scaled as a power law $\langle\langle\Delta r^2\rangle_T\rangle_{ens} \sim T^{\alpha-1}$ beyond 3 s (30 points) with $\alpha = 0.90 \pm 0.01$ for all lag times. The TEA-MSD was found to scale as $\langle\langle\Delta r^2\rangle_T\rangle_{ens} \sim t_{lag}{}^{\gamma}$ with $\gamma = 0.79 \pm 0.02$ (Fig. 3*B*). Only lag times up to 0.5 s were included in these data to avoid boundary effects (these are appreciated in the inset of Fig. 2*A*). All the previously discussed anomalous diffusion models predict the ensemble average scales as $\langle\Delta r^2\rangle_{ens} \sim t_{lag}{}^{\eta}$. The analysis presented in Fig. 3 confirms this behavior, with the exponent determined to be 0.8 ± 0.1.

Heavy-tailed CTRWs display waiting times in all scales, enabling the observation of transient channel immobilization. We identified the events in which the channel remained confined within a radius $R_{TH} \ll$ MSD and constructed the distribution of waiting times from these events. Fig. 4 shows the distributions for three different thresholds, $R^2_{TH} = 500$, 1,000, and 2,000 nm^2, which correspond to radii three, four, and six times the standard error of the mean localization accuracy (22, 32, 45 nm, respectively). Remarkably, the distribution of immobile times does not change with the threshold radius, which is consistent with a binding model. The same distribution is found for nonclustering channels.

Kv2.1 Anomalous Diffusion Is Modeled by a CTRW on a Fractal. The distributions of temporal and ensemble MSDs are consistent with the nonergodic CTRW model where the temporal averages become random quantities different from the ensemble averages (9). Noticeably, the time-ensemble-averaged MSDs exhibit aging, which can be modeled by a CTRW with a waiting-time distribution that scales as $1/\tau^{1+\alpha}$ (5, 21). The agreement between our results and the CTRW is very convincing, but both the temporal MSDs and the time-ensemble MSDs are sublinear in lag time. This is expected from diffusion on a fractal but not from a CTRW (8). In theory, the two processes can coexist, and thus we investigated the combination of a CTRW and a fractal (33, 34). Meroz et al. recently simulated a CTRW on a fractal structure (34). The ensemble-averaged MSD was found to follow a power law

$$\langle\Delta r^2(t_{lag})\rangle_{ens} = \Gamma t_{lag}^{\alpha\beta} \qquad [3]$$

where α and β are the critical exponents of the CTRW and the fractal, respectively. Due to the fractal structure, the temporal

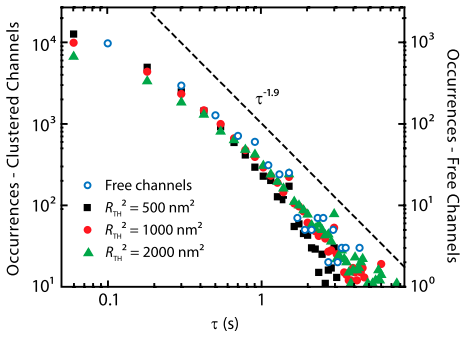

Fig. 4. Distribution of waiting times as measured using different radial thresholds. The solid symbols are from clustered channels (left axis) and the open circles from free channels (right axis). The threshold value indicates that the particle was measured to remain within that circle for the specific time. The dashed line indicates a power law $P_w(\tau) \sim \tau^{-(1+\alpha)}$ with $\alpha = 0.9$. This value corresponds to the measured MSD. At long times ($\tau > 3$ s) the distribution appears to drop faster than $\tau^{-1.9}$, suggesting a breakdown in the heavy tail of the CTRW. However, this is an artifact in our measurement, which derives from QD blinking because QDs are not in the "bright" state for that long. To verify this, we determined the probability distribution of QD "bright" times and found it to have a median of 10 s. For comparison, the figure shows a line that scales as $t^{-1.9}$, as expected from a CTRW with $\alpha = 0.9$. The distribution for clustered channels is identical to that of the free channels (○).

MSD exhibited anomalous subdiffusion $\langle \Delta r^2(t_{\rm lag})\rangle_T \sim t_{\rm lag}^{\beta}$. An additional ensemble average yielded aging and sublinearity in lag time

$$\langle\langle \Delta r^2(t)\rangle_T\rangle_{\rm ens} \sim T^{\alpha-1} t_{\rm lag}^{1-\alpha+\alpha\beta}. \quad [4]$$

These theoretical predictions agree with all our data (time MSD, ensemble MSD, and time-ensemble averages) yielding $\alpha = 0.90 \pm 0.01$ and $\beta = 0.77 \pm 0.04$. For comparison, the theoretical value of β of a walker on a percolation cluster is 0.70 and on a Sierpinski gasket is 0.86 (10).

What physical mechanisms induce a CTRW? This process can be caused by either transient binding or membrane compartmentalization. In the former model the waiting times correspond to the dissociation constant while in the latter they are related to the probability of hopping to the next compartment. The data in Fig. 4 indicate that if the CTRW corresponded to hop diffusion, the compartments would have radii smaller than 22 nm. While this is theoretically possible, such dense compartmentalization is highly improbable. Several studies have reported membrane compartmentalization in the range 140–350 nm (16, 35, 36). Lipid raft microdomains with radii as small as 20 nm have been reported (37–39), but in these cases the compartments are produced by self-association of lipids with saturated chains. Kv2.1 channels have been shown to target lipid rafts (40), and thus it is possible that the transient localization occurs within raft domains tethered to the cytoskeleton. The evidence presented here shows that the channels are either transiently immobile or localized within very small compartments because the waiting-time distribution does not change upon measuring the probability that the molecule stays within radii of 22, 32, or 45 nm. Furthermore, we found the time distribution scaled close to $1/\tau^{1.9}$, corresponding to $\alpha = 0.9$ as found from the MSDs. The same distribution is found in the single GFP trajectories showing once more that this effect is not induced by the QDs.

Effect of Actin Cytoskeleton on Kv2.1 Diffusion Pattern. We hypothesized actin plays a dominant role in Kv2.1 dynamics and investigated its effect by treating the cells with Swinholide A, a toxin that disrupts actin fibers (41). After Swinholide A application, clusters are rapidly dissolved and Kv2.1 channels become free. Strikingly, the Kv2.1 diffusion process becomes ergodic (Fig. 5*A*), but anomalous diffusion is still found (Fig. 5*C*). Individual trajectories analysis shows the CDF is anomalous and MSD is sublinear in $t_{\rm lag}$. Therefore, the mechanism underlying stationary anomalous diffusion is independent of actin filaments suggesting it is governed by interactions with macromolecular obstacles not dependent on the cytoskeleton. Similar results to those with Swinholide A were obtained with a different actin inhibitor—namely, Cytochalasin D (Fig. 5*B* and Fig. S6).

Motivated by the recovery of ergodicity, we measured the new distribution of waiting times. This distribution strongly depended on the radial threshold indicating that stationary anomalous diffusion was not related to transient binding (Fig. 5*D*). Why are there immobile episodes without transient binding? Even a Brownian walker has a finite probability of remaining within a very small radius (see *SI Text* for this derivation). The qualitative difference between a Brownian walker and a walker in a CTRW is the dependence on $R_{\rm TH}$.

The implications of our findings are clear. The actin cytoskeleton sets in action a nonstationary CTRW mechanism through a network of anchoring points. As experiments progress, Kv2.1 channels find more stable binding sites and remain on those locations for longer times. Each channel moves toward an equilibrium state and, eventually, it will find a location where it would pause for an extremely long time, such as the lifetime of the cell. In practice, this never happens. As in many physical processes in living cells, the diffusion pattern of potassium channels is actively maintained out of equilibrium. The cell constantly recycles transmembane proteins by absorbing them and sending new ones into the membrane (42). If the system were left alone—i.e., no energy was being spent on the plasma membrane—it would eventually reach a quasi-equilibrium state where all Kv2.1 potassium channels would be immobile.

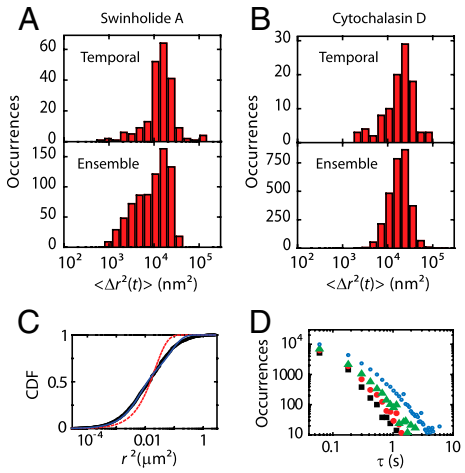

Fig. 5. Kv2.1 analysis after treatment with actin inhibitors. Channels were originally cluster-confined. After Cytochalasin D the channels remain inside clusters, but after Swinholide A, the channels become free. (*A–B*) Distribution of time-averaged (top) and ensemble-averaged (bottom) MSDs in cells treated with (*A*) Swinholide A and (*B*) Cytochalasin D. The distribution of temporal MSDs is no longer broader than the ensemble distribution. (*C*) CDF of representative trajectory after treatment with Swinholide A. (*D*) Distribution of waiting times as measured using different radial thresholds of 500 nm² (black ■), 1,000 nm² (red •), and 2,000 nm² (green ▲) in Swinholide A treated cells. For comparison, the distribution in untreated cells is also shown (blue ○).

Discussion

We found that the diffusion pattern of Kv2.1 channels is governed by a CTRW on a fractal. Naturally, these mechanisms have biological implications. Previously, it was suggested that telomere's anomalous diffusion leads to spatial chromosome organization in eukaryotes (43) and that anomalous diffusion in the bacterial cytoplasm helps transcription factors find their DNA target (44). Many transmembrane proteins are involved in cell signaling and cell-to-cell communication. For these pathways to be accurate, it is important that receptors are found rapidly. The fractal structure of the plasma membrane may be a crucial part in receptor recognition. A fractal structure increases the dimension of the random walk, and hence the same site is visited several times before the protein leaves to explore a new region. Therefore, the search for receptors is performed more carefully by a walker, minimizing the chances of missing a target in the close vicinity. On the other hand, the actin role in the CTRW suggests two different benefits for the cell. As in the case of telomeres, it favors membrane compartmentalization and organization into segregated domains. A second process that may benefit from a CTRW is endocytosis, actually the same process that keeps the CTRW running. Channels run from one anchoring point to another, but some of these may be endocytic sites from where the channel will be engulfed. Many transmembrane proteins have an intracellular domain that recognizes specific adaptor molecules and bind to them with high specificity but low affinity (45). Some of these adaptors are transiently immobile (46). Thus, the CTRW may be involved in maintaining the channel at an endocytic site so that the interaction between protein and adaptor is enhanced. Furthermore, it is observed that endocytic sites enrich specific protein concentrations (47) as expected from a CTRW-based membrane organization.

In conclusion, we have shown that the potassium channel Kv2.1 displays anomalous diffusion with a nonergodic underlying physical mechanism. A comprehensive analysis of the diffusion pattern that goes beyond MSD analysis and also includes time series analysis of individual trajectories and ensemble averages was performed. In general, single-molecule experiments provide information on particle fluctuations that average out in ensemble measurements. However, when the population is homogeneous, this information can in theory be obtained from the ensemble measurements using the fluctuation–dissipation relation. Our findings show that due to the ergodicity breaking, single-particle trajectories contain information not attainable by ensemble experiments, emphasizing the relevance of single-molecule studies. Two processes are found to coexist in the complex environment of the living cell membrane, one of them nonstationary—namely, a CTRW. The actin cytoskeleton network is found to regulate the CTRW. We propose biological implications for both mechanisms underlying anomalous diffusion. Importantly, we showed that the availability of both temporal and ensemble statistics provide enough evidence to elucidate the mechanisms associated with anomalous diffusion. A very recent report by Jeong et al. (48), showing ergodicity breaking of lipid granules in the cytoplasm of fission yeast cells, suggests that our findings may also be relevant to 3D diffusion processes.

Methods

Cell Culture and Transfection. Human embryonic kidney (HEK) 293 cells (American Type Culture Collection, passage 38-45) were cultured in DMEM, supplemented with 10% FBS, at 37 °C in a 5% CO_2 atmosphere. HEK cells were transfected with 0.5 μg/μL GFP-Kv2.1-BAD and 1.5 μg/μL BirA vectors previously described (19, 49) to express Kv2.1 channels labeled with GFP on the N-terminal domain. A biotin acceptor domain (BAD) for biotin ligase BirA was added to the extracellular region in order to tag channels with quantum dots. After electroporation, cells were plated on cover-glass-bottom culture dishes (Bioptechs) precoated with Matrigel (BD Biosciences). All cells were used for measurements within 24 h of transfection.

Total Internal Reflection Microscope. All images were acquired using an objective-type total internal reflection fluorescence microscope (TIRFM). The microscope was home-built around an Olympus IX71 body. A 473 nm laser line with 2.5 mW of power after the objective (Olympus PlanApo 100 × /1.45) was used as excitation source. A back-illuminated electron-multiplied charge coupled device (EMCCD) camera (Andor iXon DU-888) operated at −85 °C with an electronic gain of 300 was used. Simultaneous two-color imaging was achieved by optically splitting the image onto two halves of the camera, each corresponding to a separate color. Both the stage (Bioptechs) and the objective were maintained at 37 °C. Movies (>5,000 frames) were acquired using Andor IQ software at an average frame rate of eight frames per second.

Imaging Conditions. GFP-tagged Kv2.1 channels were labeled with QDs through a biotin-streptavidin biochemistry. Prior to imaging, the cells were rinsed six times with a dye-free imaging saline (146 mM NaCl, 4.7 mM KCl, 2.5 mM $CaCl_2 2H_2O$, 0.6 mM $MgSO_4$, 0.15 mM NaH_2PO_4, 0.1 mM ascorbic acid, 8 mM glucose, and 20 mM HEPES) to remove the media. The cells were incubated for 5 min in a 0.1 nM solution of streptavidin conjugated QDs (Qdot 655, Invitrogen) and 150 μM BSA (IgG- fatty-acid-free, Sigma-Aldrich) in imaging saline. Following incubation the cells were rinsed again six times with imaging saline to ensure the removal of any unbound QDs. During imaging, cells were maintained at 37 °C.

Single-Particle Tracking. QDs enabled us to track individual channels, while GFP fluorescence provided characteristics of the clusters as an ensemble. QD labeling was carefully controlled so that QDs remained at low density to allow for individual particle tracking. QDs present advantages over fluorescent proteins both in signal-to-noise ratio and in the total time an individual tracer can be followed. Individual particles were localized by fitting their fluorescence pattern to a 2D Gaussian function (50, 51). In our imaging system, the point spread function (PSF) had a standard deviation of 150 nm. Gaussian fitting was done with a custom-written algorithm in a LabView environment using Levenberg–Marquardt least squares fitting. We used a movable region of interest (ROI) and discarded trajectories that collided with each other (25% of the total number of trajectories). The localization and intensity as a function of time were determined for individual QDs. To account for blinking behavior, only QDs with intensity above a predetermined threshold were used in the analysis; all other frames were discarded. The accuracy of our tracking algorithm was determined by tracking the displacement of a QD bound to glass. The standard error of the mean (SEM) was found to be 8 nm (see *SI Text* and Fig. S7), which corresponded to an average 350 photons collected within 80 ms exposure time (51). The MSD of each trajectory was calculated in LabView by averaging over all point pairs because it was previously found to yield more accurate results than averaging independent pairs (52). Tracking and analysis algorithms are available upon request.

Actin Cytoskeleton Disruption. Actin depolymerizing drugs were used to disrupt the cytoskeletal network. Swinholide A (Sigma-Aldrich) was dissolved in DMSO and added during imaging experiments to the cells at a final concentration of 70 nM (18). Cytochalasin D (Sigma-Aldrich) was dissolved in DMSO and added to the cells while imaging, at a final concentration of 20 nM.

ACKNOWLEDGMENTS. This work was supported by the National Science Foundation under Grant PHY-0956714 and by the National Institutes of Health under Grant R01GM84136.

1. Schulzky C, Essex C, Davison M, Franz A, Hoffmann KH (2000) The similarity group and anomalous diffusion equations. *J Phys A Math Gen* 33:5501–5511.
2. Saxton MJ (1994) Anomalous diffusion due to obstacles—a Monte-Carlo study. *Biophys J* 66:394–401.
3. Zimmerman SB, Minton AP (1993) Macromolecular crowding—biochemical, biophysical, and physiological consequences. *Annu Rev Biophys Biomol Struct* 22:27–65.
4. Horton MR, Hofling F, Radler JO, Franosch T (2010) Development of anomalous diffusion among crowding proteins. *Soft Matter* 6:2648–2656.
5. Metzler R, Klafter J (2000) The random walk's guide to anomalous diffusion: A fractional dynamics approach. *Phys Rep* 339:1–77.
6. Klafter J, Blumen A, Shlesinger MF (1987) Stochastic pathway to anomalous diffusion. *Phys Rev A* 35:3081–3085.
7. Bel G, Barkai E (2005) Weak ergodicity breaking in the continuous-time random walk. *Phys Rev Lett* 94:240602.
8. Lubelski A, Sokolov IM, Klafter J (2008) Nonergodicity mimics inhomogeneity in single particle tracking. *Phys Rev Lett* 100:250602.
9. He Y, Burov S, Metzler R, Barkai E (2008) Random time-scale invariant diffusion and transport coefficients. *Phys Rev Lett* 101:058101.
10. ben-Avraham D, Havlin S (2000) *Diffusion and Reactions in Fractals and Disordered Systems* (Cambridge Univ Press, Cambridge).
11. Mandelbrot B, Van Ness JW (1968) Fractional Brownian motions fractional noises and applications. *SIAM Rev* 10:422–437.
12. Szymanski J, Weiss M (2009) Elucidating the origin of anomalous diffusion in crowded fluids. *Phys Rev Lett* 103:038102.
13. Tejedor V, et al. (2010) Quantitative analysis of single particle trajectories: Mean maximal excursion method. *Biophys J* 98:1364–1372.
14. Magdziarz M, Weron A, Burnecki K, Klafter J (2009) Fractional Brownian motion versus the continuous-time random walk: A simple test for subdiffusive dynamics. *Phys Rev Lett* 103:180602.
15. Magdziarz M, Klafter J (2010) Detecting origins of subdiffusion: p-variation test for confined systems. *Phys Rev E* 82:011129.
16. Schutz GJ, Schindler H, Schmidt T (1997) Single-molecule microscopy on model membranes reveals anomalous diffusion. *Biophys J* 73:1073–1080.
17. Deverall MA, et al. (2005) Membrane lateral mobility obstructed by polymer-tethered lipids studied at the single molecule level. *Biophys J* 88:1875–1886.
18. Tamkun MM, O'Connell KM, Rolig AS (2007) A cytoskeletal-based perimeter fence selectively corrals a sub-population of cell surface Kv2.1 channels. *J Cell Sci* 120:2413–2423.
19. O'Connell KM, Rolig AS, Whitesell JD, Tamkun MM (2006) Kv2.1 potassium channels are retained within dynamic cell surface microdomains that are defined by a perimeter fence. *J Neurosci* 26:9609–9618.
20. Scher H, Montroll EW (1975) Anomalous transit-time dispersion in amorphous solids. *Phys Rev B* 12:2455–2477.
21. Condamin S, Tejedor V, Voituriez R, Benichou O, Klafter J (2008) Probing microscopic origins of confined subdiffusion by first-passage observables. *Proc Natl Acad Sci USA* 105:5675–5680.
22. Bouchaud JP (1992) Weak ergodicity breaking and aging in disordered-systems. *J Phys-Paris* 2:1705–1713.
23. Wong IY, et al. (2004) Anomalous diffusion probes microstructure dynamics of entangled F-actin networks. *Phys Rev Lett* 92:178101.
24. Scher H, Margolin G, Metzler R, Klafter J, Berkowitz B (2002) The dynamical foundation of fractal stream chemistry: The origin of extremely long retention times. *Geophys Res Lett* 29:1061.
25. Solomon TH, Weeks ER, Swinney HL (1993) Observation of anomalous diffusion and Levy flights in a 2-dimensional rotating flow. *Phys Rev Lett* 71:3975–3978.
26. Silvestri L, Fronzoni L, Grigolini P, Allegrini P (2009) Event-driven power-law relaxation in weak turbulence. *Phys Rev Lett* 102:014502.

27. Barkai E (2003) Aging in subdiffusion generated by a deterministic dynamical system. *Phys Rev Lett* 90:104101.
28. Havlin S, Ben-Avraham D (2002) Diffusion in disordered media. *Adv Phys* 51:187–292.
29. Sung BJ, Yethiraj A (2008) Lateral diffusion of proteins in the plasma membrane: Spatial tessellation and percolation theory. *J Phys Chem B* 112:143–149.
30. O'Shaughnessy B, Procaccia I (1985) Analytical solutions for diffusion on fractal objects. *Phys Rev Lett* 54:455–458.
31. Ulbrich MH, Isacoff EY (2007) Subunit counting in membrane-bound proteins. *Nat Methods* 4:319–321.
32. Vrljic M, Nishimura SY, Brasselet S, Moerner WE, McConnell HM (2002) Translational diffusion of individual class II MHC membrane proteins in cells. *Biophys J* 83:2681–2692.
33. Blumen A, Klafter J, White BS, Zumofen G (1984) Continuous-time random-walks on fractals. *Phys Rev Lett* 53:1301–1304.
34. Meroz Y, Sokolov IM, Klafter J (2010) Subdiffusion of mixed origins: When ergodicity and nonergodicity coexist. *Phys Rev E* 81:010101(R).
35. Kusumi A, Sako Y, Yamamoto M (1993) Confined lateral diffusion of membrane receptors as studied by single particle tracking (nanovid microscopy). Effects of calcium-induced differentiation in cultured epithelial cells. *Biophys J* 65:2021–2040.
36. Sheets ED, Lee GM, Simson R, Jacobson K (1997) Transient confinement of a glycosylphosphatidylinositol-anchored protein in the plasma membrane. *Biochemistry* 36:12449–12458.
37. Schutz GJ, Kada G, Pastushenko VP, Schindler H (2000) Properties of lipid microdomains in a muscle cell membrane visualized by single molecule microscopy. *EMBO J* 19:892–901.
38. Pralle A, Keller P, Florin EL, Simons K, Horber JKH (2000) Sphingolipid-cholesterol rafts diffuse as small entities in the plasma membrane of mammalian cells. *J Cell Biol* 148:997–1007.
39. Eggeling C, et al. (2009) Direct observation of the nanoscale dynamics of membrane lipids in a living cell. *Nature* 457:1159–U1121.
40. Martens JR, Sakamoto N, Sullivan SA, Grobaski TD, Tamkun MM (2001) Isoform-specific localization of voltage-gated K+ channels to distinct lipid raft populations. Targeting of Kv1.5 to caveolae. *J Biol Chem* 276:8409–8414.
41. Bubb MR, Spector I, Bershadsky AD, Korn ED (1995) Swinholide A is a microfilament disrupting marine toxin that stabilizes actin dimers and severs actin filaments. *J Biol Chem* 270:3463–3466.
42. Trejo JA (2005) Internal PDZ ligands: Novel endocytic recycling motifs for G protein-coupled receptors. *Mol Pharmacol* 67:1388–1390.
43. Bronstein I, et al. (2009) Transient anomalous diffusion of telomeres in the nucleus of mammalian cells. *Phys Rev Lett* 103:018102.
44. Golding I, Cox EC (2006) Physical nature of bacterial cytoplasm. *Phys Rev Lett* 96:098102.
45. Owen DJ, Collins BM, Evans PR (2004) Adaptors for clathrin coats: Structure and function. *Annu Rev Cell Dev Biol* 20:153–191.
46. Doherty GJ, McMahon HT (2009) Mechanisms of endocytosis. *Annu Rev Biochem* 78:857–902.
47. Mettlen M, Loerke D, Yarar D, Danuser G, Schmid SL (2010) Cargo- and adaptor-specific mechanisms regulate clathrin-mediated endocytosis. *J Cell Biol* 188:919–933.
48. Jeon JH, et al. (2011) In vivo anomalous diffusion and weak ergodicity breaking of lipid granules. *Phys Rev Lett* 106:048103.
49. O'Connell KM, Tamkun MM (2005) Targeting of voltage-gated potassium channel isoforms to distinct cell surface microdomains. *J Cell Sci* 118:2155–2166.
50. Cheezum MK, Walker WF, Guilford WH (2001) Quantitative comparison of algorithms for tracking single fluorescent particles. *Biophys J* 81:2378–2388.
51. Yildiz A, Selvin PR (2005) Fluorescence imaging with one nanometer accuracy: Application to molecular motors. *Acc Chem Res* 38:574–582.
52. Saxton MJ (1997) Single-particle tracking: The distribution of diffusion coefficients. *Biophys J* 72:1744–1753.